

A new creep law to describe the transient and secondary creep phase

Salzer, K., Günther, R.-M., Institut für Gebirgsmechanik, Leipzig, Germany
Konietzky, H., ITASCA Consultants GmbH, Gelsenkirchen, Germany

Abstract

For stability analyses as well as for predictions of the future geomechanical behaviour of underground openings in salt rock strata, proper calculation tools are needed. Numerical calculation methods and material laws are required to describe the mechanical behaviour of salt. A proposed new material salt creep law describes the deformation-hardening behaviour of the transient creep phase, which gives a good description for a relatively short time after the excavation phase and can, by considering the recovery of the hardening, also be extended to the stationary creep phase, which is significant for long times after the creation of openings. The developed material law also includes inverse transient creep, which takes place during load reductions. This material law is used for the back-analysis of all common types of lab tests (compression, creep and relaxation) as well as for some field measurements. The material creep law was implemented into the ITASCA codes FLAC (ITASCA 1998) and FLAC^{3D} (ITASCA 1997).

1 Introduction

Since time immemorial, salt deposits have been used for the production of salt minerals. Within the last decade, the use of leaching caverns in salt rock formations for the storage of gas has become increasingly important. Also, the use of salt deposits for storing chemical-toxic and radioactive wastes have become a topic of great interest. The visco-plastic behaviour (creep) of salt rock formations leads to practical impermeability and, in the long term, to a complete sealing of openings. Therefore, the salt rock formations fulfil the demands that were made for host rock formations for underground storage caverns and repositories. For stability analyses as well as for predictions of the future geomechanical behaviour of underground openings in salt rock formations, proper calculation tools are needed. Therefore, efficient numerical calculation methods and material laws have been developed to describe the mechanical behaviour of salt.

In principle, the creep curve (i.e. the deformation-time curve (Fig. 1) under constant load), can be characterised by three phases:

- (I) a primary or transient creep phase (Hardening dominates during that part of the creep curve.);
- (II) a secondary, or stationary, creep phase during which hardening and recovery are in dynamic equilibrium; and
- (III) a tertiary, or accelerating, creep phase that involves the initiation of a creep fracture. Damage inside the rock grows more quickly than it can be repaired by relaxation and heal-up processes.

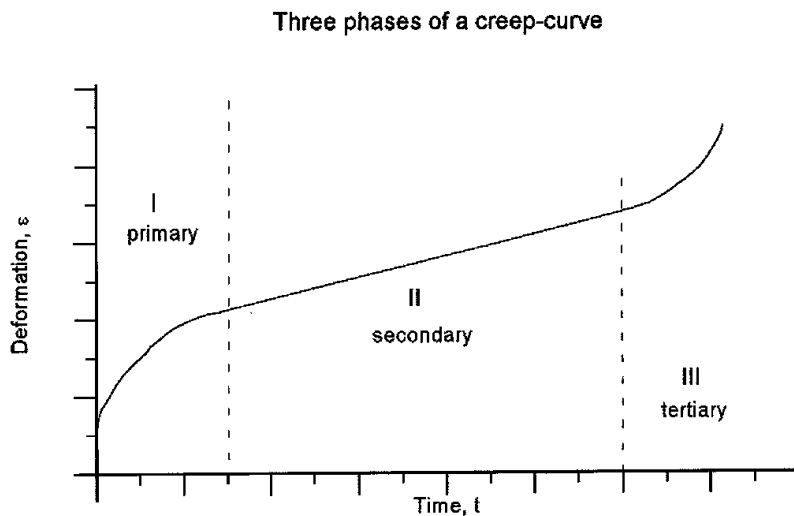


Fig. 1: The three phases of a creep curve.

The observed and measured convergence underground, especially during the phase immediately after the creation of openings, cannot be described with the secondary creep approach alone. Figure 2 shows a typical example of the measured vertical compression of a Sylvénite pillar compared to the calculated values according to the secondary creep approach (IfG 1992). The dashed bold line shows the calculated pillar compression using the secondary creep approach when the excavation time point corresponds to real time and the secondary creep parameters are fitted to the displacement velocities after 4 years. The deformation parameters for the deformation-hardening approach, which were deduced from laboratory tests in advance of pillar creation, lead to a good agreement between the in-situ measured deformations and the calculated values (see the thin line in Figure 2). For longer times, the measured values lie above the calculated ones because transition into the stationary phase has already taken place. The deformation-hardening approach with power functions for stress and deformation has been used by several authors (e.g. LEMAIRTE (1970) and MENZEL (1977)). This approach has had good success in describing the creep behaviour of salt. However, it does not include the secondary creep phase.

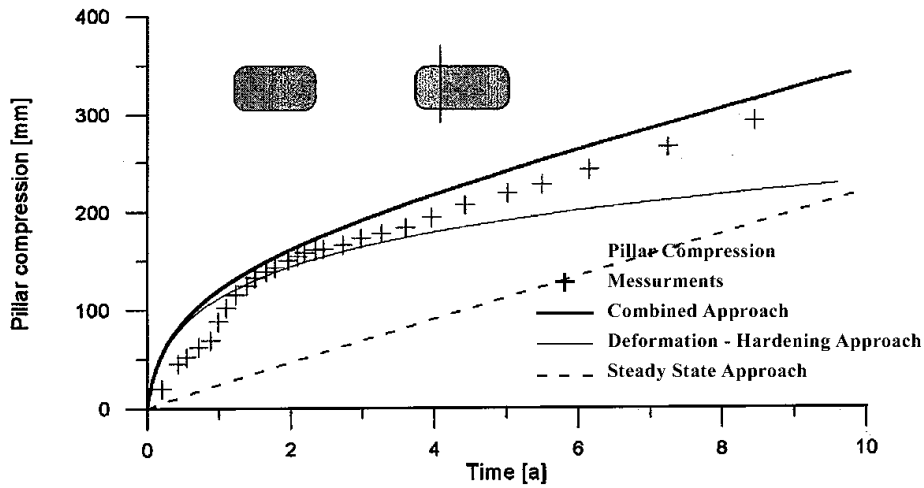


Fig. 2: Comparison between in-situ measured pillar compression and several calculated pillar compression values using different creep approaches.

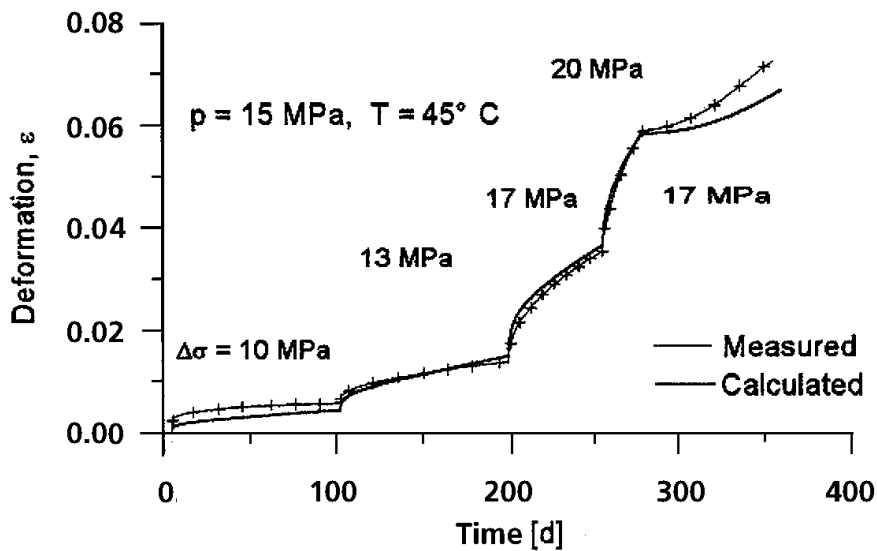


Fig. 3: The inverse transient creep demonstrated for deformation of a halite sample during a Karman test (HUNSCHE 1994).

This paper presents a new combined creep approach that contains both creep phases by recovery of the hardening, whereby the hardening-part of the creep deformation, ϵ^V , is used as an internal state variable. The inverse transient creep is also described with this creep approach. An example of the inverse transient creep that appears during the reduction of the deviatoric stresses is shown in Figure 3 (HUNSCHE 1995), which shows the deformation time curve of a triaxial test on a cylindrical salt sample in the so-called "Karman box" with 5 stress levels.

Consideration of these effects is necessary for all geomechanical processes in which the deviatoric stress level decreases (e.g. load changes in a salt storage cavern or the interaction between the salt rock and the sealing construction).

2 Mathematical description of the new material law

The strain rate tensor, $\dot{\boldsymbol{\varepsilon}}_{ij}$, is given by the following equation:

$$\dot{\boldsymbol{\varepsilon}}_{ij} = \dot{\boldsymbol{\varepsilon}}_{ij}^{el} + \dot{\boldsymbol{\varepsilon}}_{ij}^{cr} \quad (1)$$

where $\boldsymbol{\varepsilon}_{ij}^{el}$ and $\boldsymbol{\varepsilon}_{ij}^{cr}$ are the elastic and creep portions of the strain tensor, respectively. The corresponding strain rate components are:

$$\dot{\varepsilon}_{ij}^{el} = -\frac{\nu}{E} \cdot \sigma_{kk} \delta_{ij} + \frac{(1+\nu)}{E} \cdot \sigma_{ij} \quad (2)$$

$$\dot{\varepsilon}_{ij}^{cr} = \frac{3}{2} \dot{\varepsilon}_{eff}^{cr} \frac{S_{ij}}{\sigma_{eff}} \quad (3)$$

In the deformation-hardening approach, which results in a good description of the primary creep phase with non-inverse transient creep, $\boldsymbol{\varepsilon}_{eff}^{cr}$ is given by the following relation:

$$\dot{\varepsilon}_{eff}^{cr} = A^1 \frac{\sigma^{\beta^1}}{(\boldsymbol{\varepsilon}_{eff}^{cr})^\mu} \quad (4)$$

The secondary creep can be considered as a special case of this approach, with $\mu = 0$. In the proposed combined creep approach, the total creep deformation, $\boldsymbol{\varepsilon}_{eff}^{cr}$, is divided into a hardening part, $\boldsymbol{\varepsilon}_{eff}^V$ (which represents the internal state variable), and the remainder, $\boldsymbol{\varepsilon}_{eff}^R$:

$$\boldsymbol{\varepsilon}_{eff}^{cr} = \boldsymbol{\varepsilon}_{eff}^V + \boldsymbol{\varepsilon}_{eff}^R \quad (5)$$

The following equations apply in the combined approach:

$$\dot{\varepsilon}_{eff}^{cr} = A^1 \frac{\sigma^{\beta^1}}{(\boldsymbol{\varepsilon}_{eff}^V)^\mu} \quad (6a)$$

$$\dot{\epsilon}_{eff}^V = A^I \frac{\sigma_{eff}^{\beta^I}}{(\epsilon_{eff}^V)^\mu} - \frac{\epsilon_{eff}^V}{t_0} \quad (6b)$$

The second term in equation (6b) describes the recovery of that part of the deformation that acts as hardening. If the first term of equation (6b), which describes the hardening and which is equal to the growth of the total creep deformation [compare to equation (6a)] is ignored ($\sigma = 0$, total unloading of the sample), the integration of equation (6b) leads to an exponential decay of ϵ_{eff}^V with time, due to the recovering. The approach used to describe the recovery of the hardening is based on the thermal nature of this process.

For short times after the creation of the openings, and with corresponding small values for ϵ_{eff}^{cr} and ϵ_{eff}^V , the second term of equation (6b) is negligible; hence, the creep behaviour can be described by the deformation-hardening approach alone. For larger values of ϵ_{eff}^V , the importance of the second term increases. The state of stationary creep is reached if ϵ_{eff}^V does not grow further—i.e. $\dot{\epsilon}_{eff}^V = 0$. Recovery and hardening are then in dynamic equilibrium. For that creep state, the value of ϵ_{eff}^V is given by:

$$(\epsilon_{eff}^V)^{\mu+1} = (A^I \sigma_{eff}^{\beta^I} t_0) \quad (7a)$$

and the following relations apply:

$$(\dot{\epsilon}_{eff}^{cr})^{\mu+1} = A^{II} \sigma_{eff}^{\beta^{II}} \quad (7b)$$

where

$$A^{II} = A^I \left(\frac{1}{A^I t_0} \right)^{\mu+1} \quad (7c)$$

$$\beta^{II} = \frac{\beta^I}{1 + \mu} \quad (7d)$$

As will be shown later, the adjustment of t_0 to the in-situ measured deformation values gives recovery times between 10 and 20 years.

During the inverse transient creep, ϵ_{eff}^V lies above the equilibrium hardening, $(\epsilon_{eff}^V)^{\mu+1}$, for the new reduced deviatoric stress level, so that ϵ_{eff}^V reduces to a new equilibrium combined with a corresponding increase of ϵ_{eff}^{cr} as a result of the recovery process.

Due to the thermal nature of the recovery, it is reasonable to use the ARRHENIUS approach for the temperature dependence on the recovery time, t_0 :

$$t_0 = e^{\frac{Q_v}{RT}} \quad (8a)$$

Based on equation (7c), one can deduce the known temperature dependence of the secondary creep—i.e. factor A^{II} :

$$A^{II} = e^{-\frac{Q_v \mu}{RT(1+\mu)}} \quad (8b)$$

The implementation of the new creep law into FLAC and FLAC^{3D} is based on the direct numerical evaluation of the equations (6a) and (6b) for each zone and each timestep. Especially during the initial creep phase ($\epsilon_{eff}^V = 0$), extremely small timesteps are necessary. The assumption of a small primary hardening of the order of 10^{-5} accelerates the calculation process during the initial phase and shows only a negligible influence on the calculation results.

3 Validation of the new combined material law

3.1 Laboratory tests

As shown in Figure 3, the new creep law provides a good description of creep tests (load tests including multi-level creep and inverse transient creep).

The following three figures demonstrate that, with the same parameter set describing a specific salt type, the stress-deformation behaviour for three different load regimes can be reproduced. These three load regimes are: a standard creep test ($\sigma_{eff} = \text{constant}$; Figure 4), a triaxial test with constant deformation rate ($\epsilon = \text{constant}$; Figure 5) and a triaxial test with relaxation phases ($\epsilon = 0$; Figure 6).

For the halite investigated, the following material parameters were determined based on creep tests (see, for example, Figure 4):

Young's modulus = 30 GPa;	Poisson's ratio = 0,23
$A^I = 1,0 \cdot 10^{-58}$; $\beta^I = 28$;	$\mu = 7$ $t_0 = 10$ years
The system units are: σ [MPa]; t [h]	

The parallel shifting of the creep curve occurs because primary compression loading was applied in several steps in the laboratory test, and in only one step in the numerical simulation. Figure 5 shows the stress-deformation curve for a triaxial compression test

under constant deformation velocity with relaxation phases at 1% and 5% of the sample compression. Figure 6 shows the corresponding stress-time diagram. Figure 5 also documents the influence of increased deformation velocity on the stress-deformation behaviour. After the second relaxation, at a compression of 5%, the deformation velocity was increased from $5 \cdot 10^{-6} \text{ s}^{-1}$ to $2.5 \cdot 10^{-5} \text{ s}^{-1}$. An increase of the deformation velocity is connected with a stress increase at the same deformation. This is also reproduced quantitatively by the computer model.

Figure 6 shows the result of a back-analysis of both relaxation phases. The relaxation behaviour is also reproduced by the computer model with sufficient accuracy. Therefore, it can be assumed that complicated load regimes can also be modelled properly with the material model as long as the deformation has not reached the tertiary creep phase.

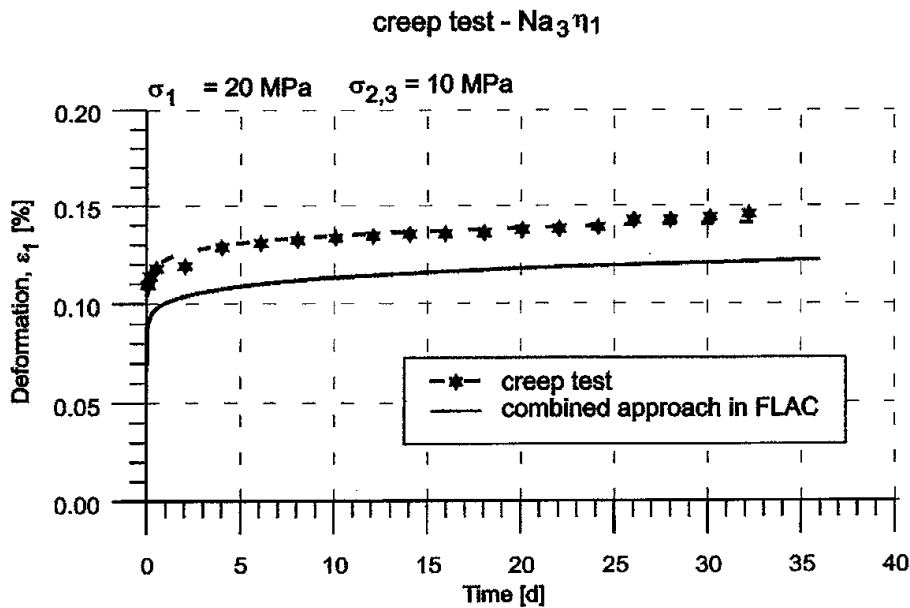


Fig. 4: Comparison between measured and calculated values for a creep test of ‘Leinsteinsalz’ (halite).

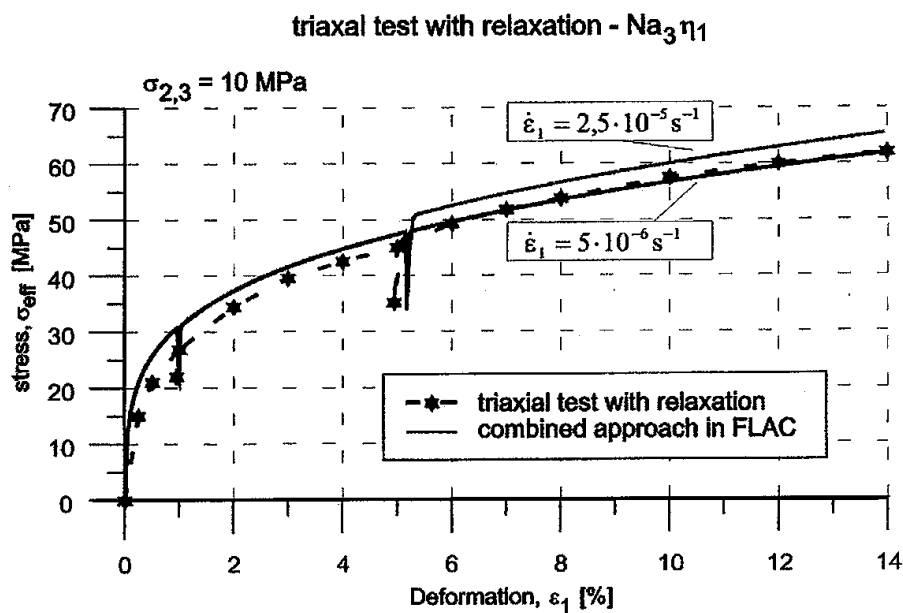


Fig. 5: Comparison between measured and calculated values for a triaxial test on ‘Leinsteinsalz’ (halite) with two interposed relaxation phases.

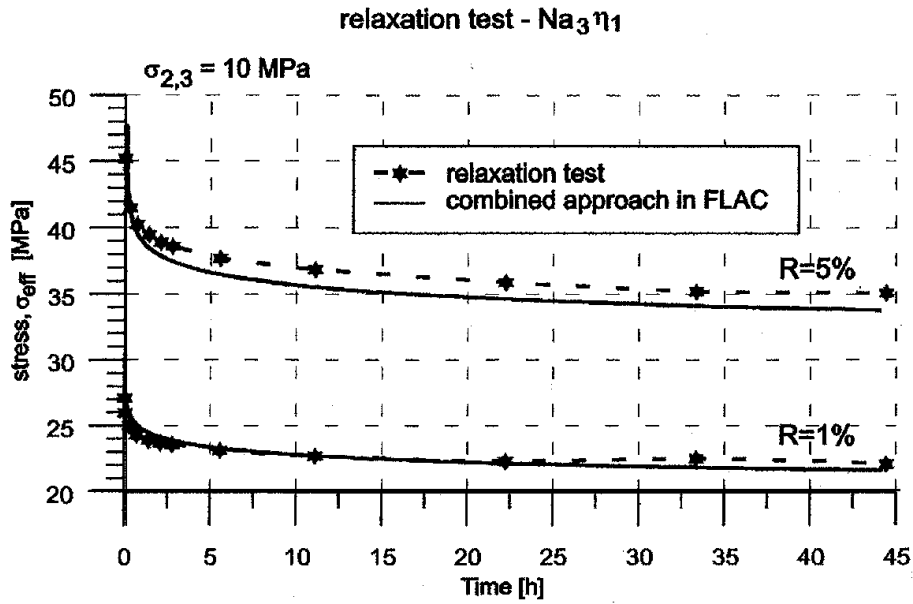


Fig. 6: Comparison between measured and calculated displacements during the relaxation phase for ‘Leinsteinsalz’ (halite).

3.2 Field measurements

With the help of the two following examples, the assessment of the recovery time, t_0 , is demonstrated. The assessment is made on the basis of the adjustment of the calculated deformation values to the in-situ measured values.

3.2.1 Sylvénite pillar

The measured in-situ pillar compression of a sylvénite pillar was compared with the calculated values (Figure 2). In this example, a quadratic pillar was transformed into a column shape that can be modelled with the axisymmetric calculation option. The zero measurement (reference) was conducted 25 days after creation of the pillar and was taken into consideration in Figure 2. With creep parameters for the deformation-hardening approach determined during the early 1970s (IFG 1992): $A^I = 1,15 \cdot 10^{-56}$; $\beta^I = 25$ and $\mu = 7,3$; the later (1978 - 1987) observed pillar compression could be described properly. Only in the last 5 years of the total measuring period did an underestimation of the pillar compression became apparent. Before investigations with the new creep approach were begun, the factor A^{II} was fitted in such a way that the pillar compression rates within the stationary phase were reproduced properly (dashed bold line). On the basis of the so-determined A^{II} , the parameter t_0 can be estimated according to equation (7c). For this example, t_0 amounts to 20,9 years. With these parameters for the combined creep behaviour, the bold line was calculated; it shows good agreement between the measured and calculated pillar compression for all considered times.

3.2.2 Salt pillar

The second example (SALZER 1996) compares calculated and measured deformation in a relatively thick salt pillar situated within a room-and-pillar system under work. The pillar width is 35 m, the room width is 20 m, and the mean pillar height is 35 m. After the excavation of a roof chamber 20-m wide and 5-m tall, the total headroom is mined by underhand stopping and hauled through a system of excavations in the floor (Figure 7).

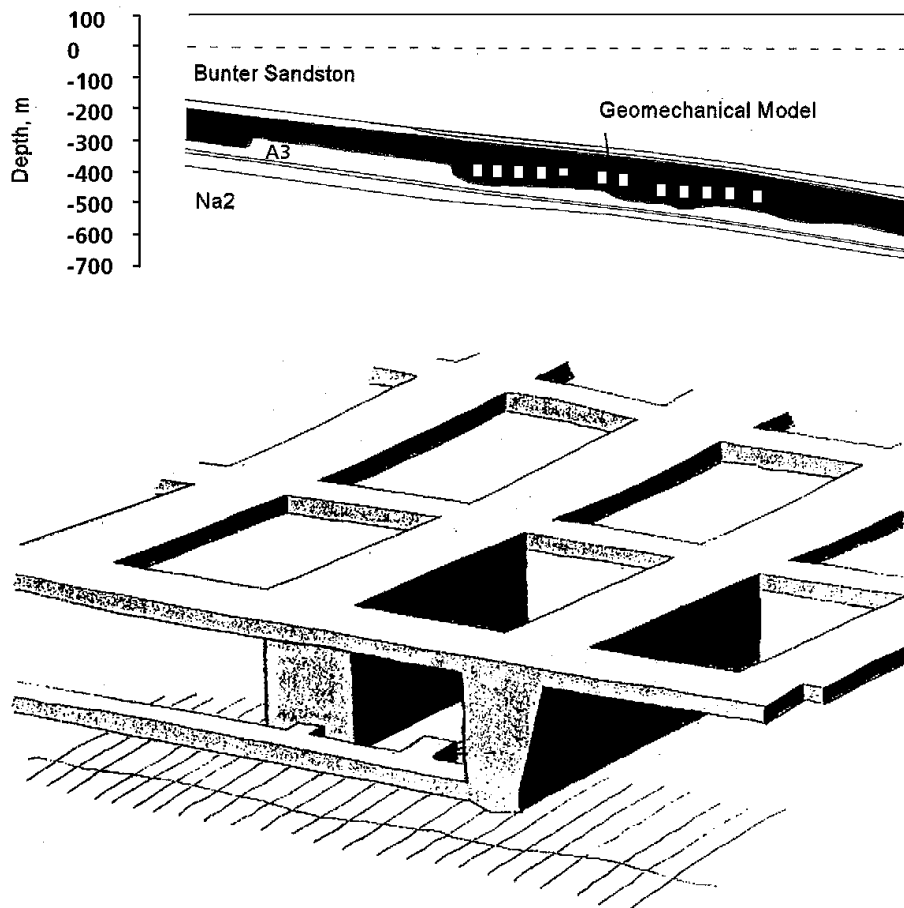


Fig. 7: Immediate surroundings of the measuring chamber (plane and perspective view).

A measuring system (MK2) was installed with the objective of monitoring the stress-deformation behaviour during the room-creation phase. The second excavation phase corresponds to the excavation of the room located Southeast 1612; the third excavation phase corresponds to the room located Northwest 1613; and the fourth phase includes the drivage of a conveyer road in the pillar itself (Figure 7). The vertical compression of the pillar and its lateral deformation is measured with 3 extensometers in boreholes; the

extensometers are oriented vertical, and horizontal into the Northeast and Northwest directions. Figure 7 shows a cross-section through the measuring plane, which serves also as the basis for the rock mechanics model. A test calculation showed that the stationary creep approach results in an unsatisfactory agreement between the in situ measured and calculated values. This is because the measurements include the creation process and, therefore, the transient creep part can not be neglected. Subsequently, the new creep approach was used, with recovery time t_0 chosen in such a way that the measured surface settlements above the mining area could be reproduced in a more complex rock mechanics model.

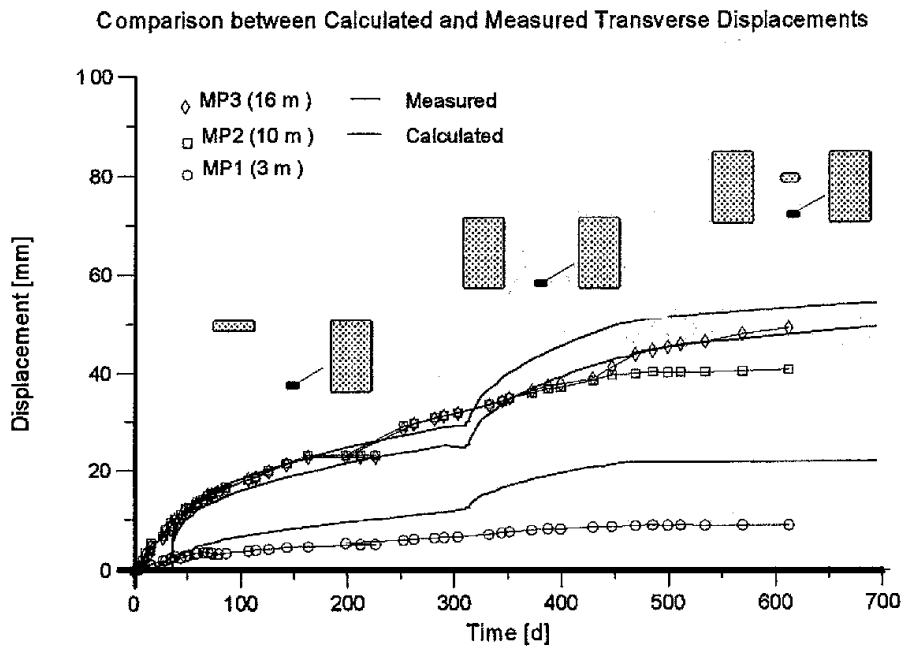


Fig. 8: Comparison between measured and calculated displacements (measuring chamber MK161/1; horizontal to slightly inclined).

The following deformation parameters were chosen:

$$\begin{array}{lll} \text{Young's modulus} = 25 \text{ GPa} & \text{Poisson's ratio} = 0,25 & \mu = 1,6 \\ A^I = 1,7 \cdot 10^{-22}; & \beta^I = 10; & t_0 = 10 \text{ years} \end{array}$$

Figure 8 shows a comparison between the calculated and measured displacements which were obtained from the measuring chamber. It also shows a comparison for the displacements between the control points inside the measuring chamber and points at distances of 3, 10 and 16 m from the chamber periphery. The calculated values for the 10-m and 16-m measuring lines show good agreement with the measured values; for the 3-m measuring line, the 3-dimensional effect of the chamber face becomes important. The calculated minor principal stresses correspond quite well with the shut-in pressure values obtained from hydraulic fracturing measurements.

4 Conclusions

The proposed new combined creep law, which is implemented into the codes FLAC and FLAC^{3D}, allows a proper description of the secondary, transient and inverse transient creep phases. The proposed combined creep law corresponds to the addition of a new component in the deformation-hardening model formulation to account for a better description of the transient creep phase by consideration of hardening recovery and allow modelling of secondary creep phase and inverse creep. The examples presented show good agreement between the measured and calculated deformations and for the new calculated values according to the new combined creep approach, although the deduced creep parameters, A^I , b^I and m were already determined on the basis of load tests before the excavation had taken place and only recovery time t_0 was adjusted to the in-situ measurements. A first assessment of t_0 under mining temperature conditions (30° C) gives values between 10 and 20 years

5 Acknowledgement

The presented work was granted by the Federal Ministry of Research and Technology under the contract 02-C0062-8.

6 Literature

Hunsche U., Schulze, O. :

Personnel communication, (1995).

IfG:

Überprüfung vorhandener Modellvorstellungen zum Konvergenzverhalten und zur Standsicherheit komplexer Grubengebäude im Salzgestein. Forschungsvorhaben BMFT-FB/02 E 8161 6, IfG GmbH Leipzig, Januar 1992, (1992).

ITASCA Consulting Group, Inc.:

FLAC^{3D}, Version 2.0, Minneapolis, Minnesota: ICG. (1997).

ITASCA Consulting Group, Inc.:

FLAC, Version 3.4, Minneapolis, Minnesota: ICG. (1998).

Lemaitre J.:

Sur la détermination des lois de compartement des matériaux. *ela viscoplastiques*, thesis, Public., O.N.E.R.A N° 135 81970), Paris, (1970).

Menzel W., Schreiner W.:

Zum geomechanischen Verhalten von Steinsalz verschiedener Lagerstätten der DDR. Teil II: Das Verformungsverhalten, *Neue Bergbautechnik* 5, 8: 565 - 571, (1977).

Salzer K., Schreiner W.:

Long-term safety of salt mines in flat beddings. 4th Conference on the Mechanical Behavior of Salt, Montreal, (1996)